Desalination 376 (2015) 94–108

Contents lists available at ScienceDirect

Desalination

journal homepage: www.elsevier.com/locate/desal

Experimental and theoretical investigation on water desalination using air gap membrane distillation

A. Khalifa [a,*], D. Lawal [a], M. Antar [a], M. Khayet [b,c]

[a] King Fahd University of Petroleum & Minerals, Mechanical Engineering Department, Dhahran 31261, Saudi Arabia
[b] Department of Applied Physics I, Faculty of Physics, University Complutense of Madrid, Av. Complutense s/n, 28040 Madrid, Spain
[c] Madrid Institute for Advanced Studies of Water (IMDEA Water Institute), Calle Punto Net No. 4, Alcalá de Henares, 28805 Madrid, Spain

HIGHLIGHTS

- Comprehensive experimental and theoretical studies on AGMD
- Effects of main operating and design variables
- Feed temperature and air gap width are main controlling variables
- Theoretical results agree with experimentally measured values
- Evaporation efficiency and temperature polarization are investigated

ARTICLE INFO

Article history:
Received 9 May 2015
Received in revised form 17 August 2015
Accepted 20 August 2015
Available online 5 September 2015

Keywords:
Water desalination
Air gap membrane distillation (AGMD)
Performance evaluation
Experimental investigation
Theoretical modeling
Efficiency analysis

ABSTRACT

Membrane Distillation (MD) is a thermally driven membrane separation technique that is used for water desalination by separating water vapor from feed salty/brackish water using micro-porous hydrophobic membrane. Comprehensive experimental and theoretical studies on the performance of an air gap membrane distillation (AGMD) system are presented. The effects of main operating and design variables on the permeate flux are reported. The design of the AGMD module and the experimental setup are presented in details. PTFE membranes of two different pore sizes are characterized and tested. Results show that the system performance is highly affected by changes in both feed temperature and air gap width. Increasing the feed temperature from 40 °C to 80 °C increases the flux by 550% to 750%, depending on the other operating variables. A maximum of 130% rise in flux, approximately, was achieved when the air gap width was decreased from 7 mm to 3 mm. The maximum permeate flux obtained from the current AGMD system is 71.1 kg/m^2 hr. The measured salt rejection factor is above 99.9% that emphasizes the suitability of the AGMD system for desalination of high concentration feeds. A theoretical model based on the analysis of heat and mass transfer is developed to predict the permeate flux and to study the system efficiency. The theoretical model is validated by comparing the permeate flux with experimentally measured values where a maximum deviation of 15% is observed. The evaporation efficiency of the AGMD module and the temperature polarization coefficient are thoroughly investigated theoretically at different operating parameters.

1. Introduction

Due to urbanization and population rise, the gap between the demand and supply of potable water is ever increasing. In some arid and semi-arid areas, desalination remains the viable solution to water scarcity problem. The market for water desalination is increasing in Gulf Cooperation Council (GCC) countries as the populations grow, drought conditions worsen, and water demand per capita increases [1]. The quest for more and better fresh water production has consistently put researchers in search for superior and most efficient potable water production technology. The emergence of Membrane Distillation (MD) technology contributed in the research for seawater desalination. Membrane distillation differs from other membrane technologies in the sense that the driving force for permeation is the vapor pressure difference, rather than the total pressure of water across the membrane. The membrane materials used for membrane distillation are hydrophobic in nature. Since MD has the theoretical ability to attain 100% salt rejection and can be operated at low temperatures (40 °C–90 °C) and at atmosphere pressure, low-grade energy like solar and waste energy can be used for MD water desalination [2].

* Corresponding author.
E-mail address: akhalifa@kfupm.edu.sa (A. Khalifa).

http://dx.doi.org/10.1016/j.desal.2015.08.016
0011-9164/

Air gap membrane distillation (AGMD) has been used for seawater desalination. In an AGMD configuration, the temperature difference across the hydrophobic membrane creates partial pressure difference which encourages water molecules to evaporate at the hot feed side to permeate through the membrane pores. The vaporized water then diffuses through a stagnant air gap situated between the membrane and a condensation plate where it condenses at a lower temperature to produce distilled water [3]. Factors affecting the performance of air gap membrane distillation were investigated experimentally by several researchers. However, many inconsistencies in results are found in the open literature regarding the performance of the AGMD system (e.g. values of flux and behavior trends). Pangarkar and Sanean [4] experimentally investigated the performance of air gap membrane distillation for aqueous NaCl solution, natural ground water and seawater. The effect of operating parameters such as the feed flow rate, the feed temperature, the feed salt concentration, the coolant temperature and the air gap thickness on the permeation flux was studied. Scale deposits observed on the membrane surface reduced the permeate flux by about 60% and 23% when the both natural seawater and ground water were used as feed solutions. Using two-hollow-fiber-sets based compact membrane device, Singh and Sirkar [5] experimentally investigated influence of operating parameters and membrane types and properties on the performance AGMD system.

In order to enhance the performance of the AGMD system, Tian et al. [6] presented an innovative design of an AGMD system. The new design of AGMD configuration was reported to have significantly enhanced water productivity of the system. The AGMD module was built in such a way that the membrane material is in partial contact with the condensation surface. The transport resistance of the air gap was reduced hence improving the system efficiency. A maximum permeate flux of 119 kg/m^2 hr was reported. In an effort to improve the performance of AGMD unit, Khalifa [7] built and tested a module that can have either an air gap or a water gap. It was reported that the increase in flux ranges between 90% and 140%, depending on the feed temperature, when using the water gap as compared to the air gap. The temperature inside the water gap is lower than that of the air gap under the same operating conditions. Other researchers have also made similar attempts to improve the performance of AGMD by replacing air in the gap with liquid [8,9] with significantly different results. Bahar et al. [10] enhanced the system performance by about 50% by replacing the flat coolant plate with channeled one, which improved the heat transfer during condensation. The effect of membrane pore size on permeate flux was investigated [11]. In general, it was reported that membranes with larger pore size produce higher permeate flux. Lawal and Khalifa [12] studied the performance of double-stage AGMD unit at different operating parameters such as feed temperature, feed flow rate, coolant temperature, coolant flow rate and air gap width. Experimental results revealed that the double-stage AGMD unit is capable of achieving a maximum cumulative distillate production of 128.46 kg/m^2 hr, and a single stage flux of 65.81 kg/m^2 hr.

Dehesa-Carrasco et al. [13] investigated the performance of an AGMD unit both experimentally and theoretically. The system was manufactured from an insulated material to minimize heat losses. With the help of temperature and flow rate measurement, the enthalpy and the diffusion coefficient of vapors in the air gap were evaluated. The model predictions and the experimental data showed good match. The differences between measured and predicted temperatures were approximated to 5% accuracy. However, the trends of the model and the experimental data were different and the possible improvements to the model were discussed. Alsaadi et al. [14] developed a one dimensional model based on theoretical equations governing the mechanism for mass and heat transfer process in AGMD. The developed model is reported to be capable of predicting flux in both AGMD modules in counter-current and co-current flow regimes. The model was validated against the experimental data. Comparison showed that the model flux predictions are strongly correlated with the experimental data, with model predictions being within +10% of the experimentally determined values. Then, the model was subsequently used to study and analyze the thermal efficiency and the parameters that improved the AGMD unit. Geng et al. [15] developed an AGMD module with internal heat recovery for water desalination to investigate the impact of AGMD operating parameters. Based on mass and energy balance, a theoretical model was developed to estimate the permeate flux and temperature drop along the membrane. Results revealed that higher permeate flux and temperature drop were observed at the upper part of the module when compared to that of the lower part. Experimental results yielded maximum permeate flux of 5.3 kg/m^2 hr and a gain output ratio of 5.7.

In this paper, detailed experimental and theoretical investigations on the performance of AGMD system for water desalination are presented. Detailed experiments are conducted to provide better understanding of the factors influencing air gap membrane distillation process. A theoretical analysis of heat and mass transfer inside the AGMD module is used to predict the system permeate flux. The theoretical model is validated against the experimental findings. The evaporative (thermal) efficiency and temperature polarization of the system are calculated and discussed at different operating conditions.

2. Theory

Heat and mass transfer take place simultaneously inside the AGMD module. The analysis of heat and mass transfer in AGMD involves convective heat transfer from hot feed solution to the membrane surface, evaporation at the membrane pores' entrance liquid-gas interface, movement of water vapor across the membrane pores, conductive heat transfer across membrane material, water vapor diffusion via the stagnant air gap, vapor condensation over the cooling plate, conductive heat transfer across the condensation plate, and convective heat transfer from cold solution to the condensation plate [16]. Fig. 1 shows a schematic for the heat and mass transfer inside the AGMD module. In modeling the AGMD, the following assumptions are considered: steady state conditions, air trapped within the membrane pore is considered stagnant, constant pressure inside the air gap, and liquid entrance pressure is greater than the pressure at the feed side of the membrane. Within the air gap, mass is transported by diffusion while heat is transferred by conduction and no heat exchange between the system and the surrounding. A film-wise condensation in the air gap is considered on the condensation plate.

2.1. Heat transfer

Referring to Fig. 1, at steady state operation, the heat flux (W/m^2) from the hot solution to the membrane surface is made up of convective term and the diffusive term, given as [2,17,18]:

$$Q_f = (h_f + J_w C_{p,f})(T_f - T_{mf}) \quad (1)$$

where J_w is the permeate flux, h_f is the feed heat transfer coefficient, and $C_{p,f}$ is the specific heat of the feed solution. The convective term is dominant over the heat transfer associated with the mass transfer term in Eq. (1).

The heat transfer from membrane surface to the condensate liquid interface is expressed as:

$$Q_p = h(T_{mf} - T_{cd}) + J_w H_w \quad (2)$$

where H_w is enthalpy of vaporization of water (kJ/kg), which may be calculated from [2,26] as:

$$H_w = 1.75535\boldsymbol{T} + 2024.3 \quad (3)$$

where T is the absolute temperature in K.

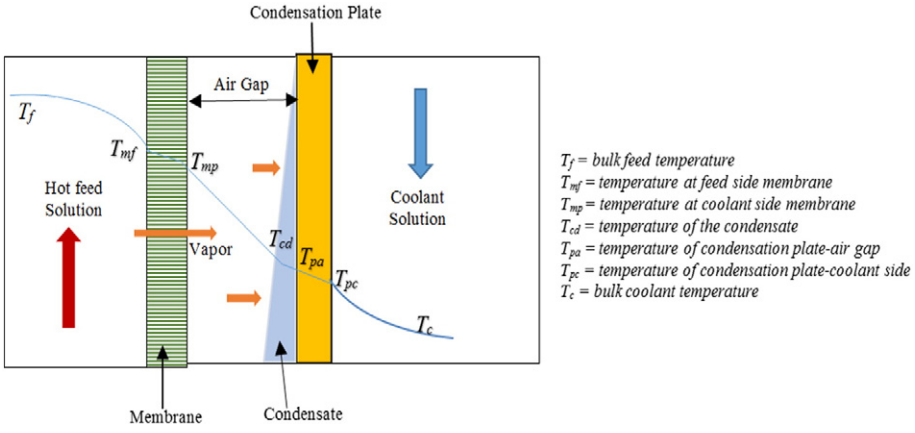

Fig. 1. Schematic for the heat and mass transfer inside the AGMD module.

The heat transfer coefficient h. Eq. (2) is expressed as [2,17]:

$$h = \left(\frac{J_w C_{cd}}{1-e^{-\frac{J_w C_{cd}}{h_y}}}\right). \tag{4}$$

C_{cd} and h_y are the specific heat and the coefficient of heat transfer co-efficient in the gaseous phase but $h_y = \frac{k_y}{b}$, where k_y is the gas phase thermal conductivity, and b is the air gap width.

The heat transfer from condensation layer interface to the cooling solution is expressed as [2]:

$$Q_c = h_d(T_{cd}-T_{pa}) = \frac{k_c}{l}(T_{pa}-T_{pc}) = h_c(T_{pc}-T_c) = h_p(T_{cd}-T_c) \tag{5}$$

where h_d is the heat transfer coefficient of the condensate, k_c is the condensation plate thermal conductivity, l is plate thickness, h_c is the heat transfer coefficient of coolant film and h_p is the overall heat transfer co-efficient from vapor/condensate liquid interface to cooling solution and it is expressed as [2,23]:

$$h_p = \left(\frac{1}{h_d}+\frac{l}{k_c}+\frac{1}{h_c}\right)^{-1} \tag{6}$$

and

$$h_d = \left(\frac{g\rho^2 H_w k_p^3}{L\mu_d(T_{cd}-T_{pa})}\right)^{\frac{1}{4}} \tag{7}$$

where ρ, k_p and, μ_d are the fluid density, thermal conductivity and dynamic viscosity at the condensate film temperature respectively, L is the height of condensation plate (or air gap) and g is the acceleration due to gravity.

Manipulating and solving Eqs. (1) to (5) lead to:

$$T_{mf} = T_f - \left(\frac{\left(\frac{1}{h_f}+\frac{1}{h}+\frac{1}{h_p}\right)^{-1}}{h_f}\right)\left((T_f-T_c)+\frac{J_w H_w}{h}\right) \tag{8}$$

and

$$T_{cs} = T_c + \left(\frac{\left(\frac{1}{h_f}+\frac{1}{h}+\frac{1}{h_p}\right)^{-1}}{h_f}\right)\left((T_f-T_c)+\frac{J_w H_w}{h}\right). \tag{9}$$

The heat transfer coefficients (h_f and h_c) may be estimated from the empirical correlation of the dimensionless numbers expressed as [2,19].

For laminar flow, the Nusselt number, Nu, correlation is given by

$$Nu = 1.86\left(Re\ \ \mathrm{Pr}\frac{d}{L}\right)^{0.33} \tag{10}$$

where $Nu = \frac{hD_h}{k}$, Pr is the Prandtl number expressed as $\mathrm{Pr} = \frac{\mu C_p}{k}$, Re is the Reynolds number given by $Re = \frac{\rho V D_h}{\mu}$, and D_h is the flow channel hydraulic diameter.

For turbulent channel flow, the following expression may be used [2,27,28]:

$$Nu = 0.023\,Re^{0.8}\ \ Pr^{0.33}\left(\frac{\mu_b}{\mu_{ms}}\right)^{0.14} \tag{11}$$

where μ_b and μ_{ms} are the water dynamic viscosity at the bulk feed temperature and at the membrane surface temperature; respectively. Other Correlations for estimating heat transfer coefficient can be found in [19,20].

2.2. Mass transfer

The mass transfer across the membrane depends on the vapor pressure difference between sides of the membrane. The relationship between mass transfer and water vapor pressure difference in AGMD is given as [2,19,21,29,30]:

$$J_W = B_w\,(P_{mf}-P_{cd}) \tag{12}$$

where P_{mf} is the vapor pressure at the feed side of the membrane, while P_{cd} is the vapor pressure at the condensate/condensation surface interface. The vapor pressure may be estimated from Antoine equation as [2]:

$$P_v(T) = \exp\left(23.1964-\frac{3816.44}{T-46.13}\right) \tag{13}$$

If one considers the effect of salts concentration in the feed solution then Eq. (12) can be modified as,

$$J_W = B_w\left(\gamma_{wf}.x_{wf}.P_{mf}-P_{cd}\right) \tag{14}$$

where γ_{wf} is activity coefficient and x_{wf} is the water mole fraction of the feed solution.

For an aqueous solution of NaCl, the activity co-efficient is given as

$$\gamma_{wf} = 1-(0.5x_{NaCl})-(10x^2{}_{NaCl}) \tag{15}$$

where x_{NaCl} is the mole fraction of $NaCl$ in water solution. It is worth quoting that for dilute feed aqueous solutions, the well-known Raoult's law may be applied to determined the vapor pressure of water [3].

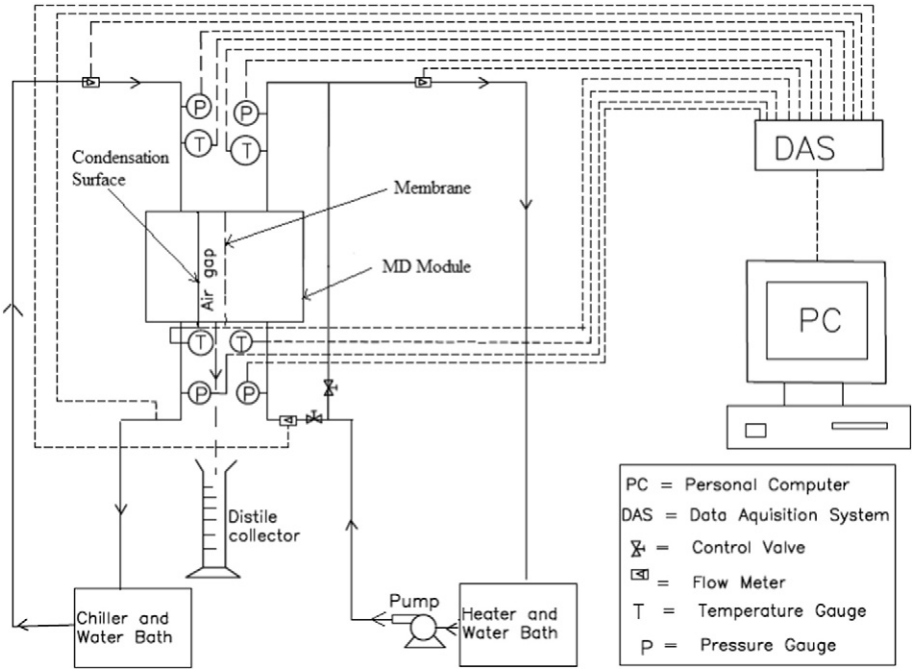

Fig. 2. Schematic line diagram of the experimental setup.

The overall mass transfer coefficient (B_w), also known as membrane permeability, given in Eqs. (12) and (14) can be evaluated as [2]:

$$B_w = \frac{\varepsilon P D_{wa}}{RT(\delta\tau + b)|p_a|_{\ln}} \tag{16}$$

where ε is the membrane porosity, P is the total pressure inside the pore, D_{wa} is the diffusion coefficient of water vapor into the air, R is the gas constant, T is the absolute temperature, δ is the membrane thickness, τ is the membrane tortuosity, b is the air gap width.

$|\mathrm{Pa}|_{\ln}$ is the log mean air pressure expressed as:

$$|p_a|_{\ln} = \frac{\left(p_{a,mf} - p_{a,cd}\right)}{\ln\left(\frac{p_{a,mf}}{p_{a,cd}}\right)}. \tag{17}$$

The product term PD_{wa} in Eq. (16) is given as [2,26]:

$$PD_{wa} = 1.895 \times 10^{-5} T^{2.072}. \tag{18}$$

Alternatively, the diffusion coefficient of water vapor into the air may be obtained from the following expression [22,23]:

$$D_{wa} = D^c \left[\frac{T}{298}\right]^{2.334} \tag{19}$$

where D^c is the mass diffusivity between the air and water vapor.

The membrane tortuosity is calculated as [31,32]:

$$\tau = \frac{1}{\varepsilon}. \tag{20}$$

2.3. Polarization coefficients and thermal efficiency

Temperature polarization coefficient, *TPC*, is commonly used to measure the extent of resistance of boundary layer over the resistance of total heat transfer. It is expressed as [2]:

$$\theta = \frac{T_{mf} - T_{cd}}{T_f - T_c}. \tag{21}$$

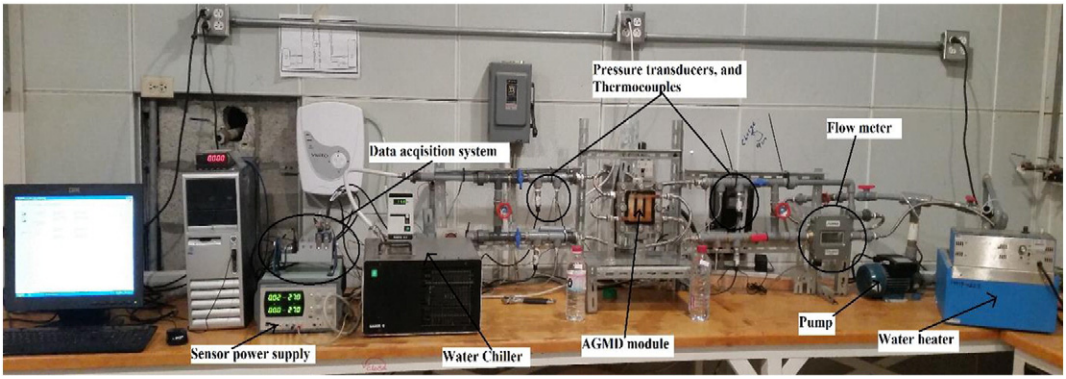

Fig. 3. A photograph of the actual laboratory setup and its components.

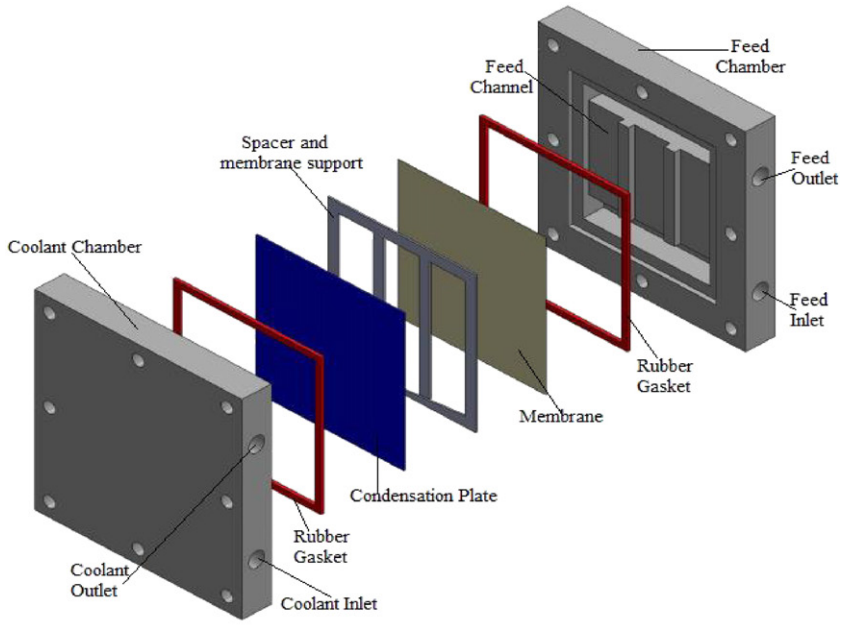

(a) An exploded view of the AGMD module assembly

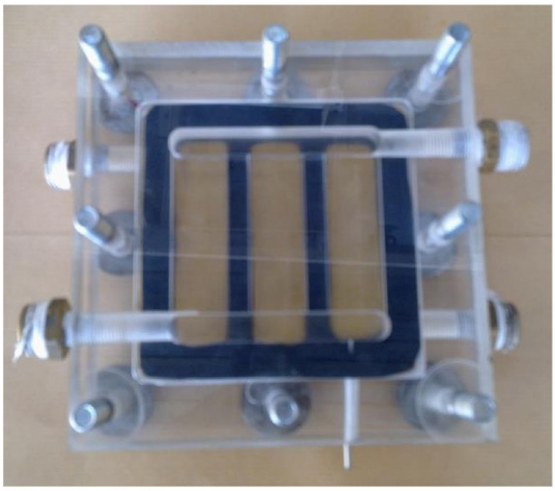

(b) A photograph of the actual module

Fig. 4. Details of the AGMD module. (a) An exploded view of the AGMD module assembly. (b) A photograph of the actual module.

Table 1
Characteristics of the used PTFE membranes (δ: total thickness; δ_{PTFE}: thickness of the PTFE top layer; d_p: mean pore size; ε: porosity; τ: pore tortuosity; θ_{PTFE}: water contact angle of the PTFE top layer; θ_s: water contact angle of the support, *LEP*: liquid entry pressure).

Properties	PTFE 0.22 μm	PTFE 0.45 μm
δ (μm)	159.5 ± 18.0	153.9 ± 13.6
δ_{PTFE} (μm)	7.9 ± 1.8	6.9 ± 2.0
d_p (nm)	236 ± 6	379 ± 8
ε (%)	75.9 ± 5.4	79.7 ± 8.7
τ[a]	1.3	1.3
θ_{PTFE} (°)	138.3 ± 2.4	139.0 ± 2.8
θ_s (°)	121.4 ± 3.4	119.3 ± 1.0
LEP (bar)	3,5 ± 0,1	2,6 ± 0,1

[a] The tortuosity factor was calculated using ($\tau = 1/\varepsilon$) [33,34].

The value of temperature polarization coefficient is given by the temperature difference between the evaporation surface and the condensation surface divided by the bulk temperature difference between the feed and the permeate [25].

The concentration polarization coefficient is defined as [2]:

$$\eta = \frac{C_{mf}}{C_f} \tag{22}$$

where C_{mf}, and C_f are the salt concentrations at the feed membrane surface and bulk feed solution, respectively.

The Evaporation (Thermal) Efficiency, *EE*, of the AGMD system is expressed as [2]:

$$\mathrm{EE} = \frac{Q_v}{Q_v + Q_c} \times 100\% \tag{23}$$

where Q_v is the heat of the vaporized liquid which is expressed as $Q_v = J_w H_w$, and Q_c is the heat transfer by conduction via the membrane and the air gap. The conduction heat lost from the feed to the permeate in AGMD may be expressed as:

$$Q_c = \frac{(T_{mf} - T_{cd})}{\frac{\delta}{K_m} + \frac{b}{K_g}} \tag{24}$$

where δ. the membrane thickness, K_m is the effective thermal conductivity of the membrane material and the gas filling its pores. K_m can be estimated from the Iso-stress model given by [2,24]:

$$K_m = \left[\frac{\varepsilon}{K_g} + \frac{(1-\varepsilon)}{K_p}\right]^{-1} \tag{25}$$

where K_g and K_p are the thermal conductivities of the gas filling the membrane pores and membrane material; respectively.

The salt rejection factor (R_f) is calculated from the following relation [2,3,4,24]:

$$R_f = \left(\frac{C_f - C_p}{C_f}\right) \times 100\% \tag{26}$$

where C_f *and* C_p are the salt concentrations of the feed water and permeate, respectively.

The above-mentioned heat and mass transfer equations were solved simultaneously using the Engineering Equation Solver (EES) software, which can solve a closed set of equations and perform automatic iterations based on initial guess values until the solution converges. Detailed theoretical analysis of the AGMD module is presented by Lawal [33].

3. Experimental work

3.1. Description of setup

An experimental lab-scale setup was constructed with a channeled AGMD module, which includes a flat sheet membrane, to investigate the MD system performance under different operating conditions. A schematic line diagram of the setup is shown in Fig. 2 and a photograph of the actual setup is shown in Fig. 3. The feed saline water is heated to the required temperature using a thermostat water circulation bath (model: HAAKE D8-G) and is pumped to the membrane cell (module) using a small centrifugal pump. The hot feed passes over the hydrophobic membrane surface and returns to the feed container. Coolant water temperature is controlled and flow is circulated using a refrigerated water bath circulator (model: HAAKE-GH). The air gap width is determined and changed by the thickness of the rubber gasket installed between the membrane and the condensation plate. Condensation takes place on a 1.5 mm-thick brass plate.

Each of the two cycles, the hot feed water cycle and the coolant water cycle, is equipped with two thermocouple probes (model: Omega TC-K-NPT-U-72) to measure the stream temperature at the module inlets and outlets, two pressure transducers (model: Omega PX309-015G5V) to measure the pressure at the module inlets and outlets, and one flow meter (model: Omega FPR302 flow meter with DPF 701 display) to measure the cycle flow rate. All the measuring devices and sensors are connected to the National Instrument (NI) data acquisition system (USB IN 9211 and IN 9234 modules) and all measured values are monitored and stored on a computer using a Labview code. The pump has a fixed speed and thus a by-pass line is installed in the feed line to control the feed flow rates with the help of control valves. The permeate is collected from the bottom of the module air gap via a small tube where its volume is recorded. The permeate concentration (Total Dissolved Solids, TDS and the Electric Conductivity, EC) of both feed water and the distillate are measured with Omega CDH-287 conductivity meter. In order to calculate the permeate flux; the sample time is recorded for each experiment. Permeate flux is then calculated by dividing the mass of collected permeate by the product of membrane effective area and sample time duration. The solutions used as feed water include distillate water, laboratory prepared salt-water (NaCl solutions) with different concentrations of 4, 10, 20, 30, 40, and 50 g/L, and raw seawater having TDS value of 60 g/L; which was directly obtained from the Arabian Gulf Sea, the city of Khobar, Saudi Arabia.

The module (sometimes referred to as membrane cell) is mainly composed of two compartments, made of Plexiglas material, to host the hot feed water and the coolant flow channels. Each compartment has three flow channels with channel dimensions of 22 mm width, 6 mm depth, and length of 70 mm. The effective membrane permeation area is $2.29 \times 10^{-3} m^2$. An exploded view of the module components is shown in Fig. 4. The rubber gaskets help in sealing the flow channels and also preventing the damage of membrane material at the sharp edges of the module when applying pressure by bolts. The membrane support holds the membrane from deflection under the feed pressure and determines the gap width. The gap width is varied by attaching different gaskets to the membrane support plate.

3.2. Membranes characterization

The membranes used are commercial polytetrafluoroethylene (PTFE) composite sheets of 0.45 μm and 0.22 μm pore sizes (PTFE 0.45 μm and PTFE 0.22 μm), and were acquired from Tisch Scientific company. The membrane sheets have an active layer and a support layer. In order to determine the membrane parameters, various characterization techniques are employed. Membranes characterization was conducted in the department of Applied Physics I, University Complutense of Madrid (UCM), Spain, and the measured membrane properties are listed in Table 1. The total thickness of the membrane (δ) and that of the PTFE top layer (δ_{PTFE}) was measured at different points of each sample by an electronic micrometer Schut (Schut Geometrical Metrology) and the average values together with their standard deviations were calculated as reported in Table 1. The mean pore size was determined at room temperature using a porometer (POROLUX™ 100) with a pressure range from 0 to 0.7 MPa. POREFIL 125 (Porometer) was used as a wetting liquid agent. At least, three different measurements are taken and the mean pore size of each tested membrane sample is reported. The porosity (ε) of each membrane was determined by measuring the density of the membrane using isopropyl alcohol (IPA) and distilled water at room temperature. The applied method was reported in details by Khayet and Matsuura [2]. In this method, a Pycnometer and a digital balance having an accuracy of 0.00001 g was used. At least, eight different measurements were taken and the average ε value of the membrane and its standard deviation were calculated. The water contact angles of the membrane PTFE top layer (θ_{PTFE}) and the supporting layer (θ_s) were measured at room temperature by a computerized optical system CAM200, equipped with CCD frame grabber camera and image analysis software. The contact angle measurements were performed at both left and right sides of each drop and were automatically calculated by fitting the captured drop shape to that obtained from Young-Laplace equation. Five drops and five readings (one per second) per drop were obtained and the average values were calculated and reported together with their standard deviations.

4. Results and discussion

4.1. Comprehensive experimental results

In this section, the impacts of the AGMD operating and design parameters on the system flux are presented. The influences of feed temperature, coolant temperature, feed flow rate, coolant flow rate, air gap width, membrane pore size, feed concentration, and performance

degradation with time, on the permeate flux are discussed. The test conditions upon which the experiment was conducted are presented below each figure.

4.1.1. Effect of feed temperature on permeate flux

Fig. 5 illustrates the effect of feed temperature on the permeate flux at different coolant temperatures. Increasing the feed temperature leads to exponential rise in the permeate flux. The reason is best explained by Antoine equation (Eq. (13)) which shows that the effect of temperature on vapor pressure is considerably low at low feed temperatures and becomes significant at higher feed temperatures. Furthermore, since the vapor pressure depends exponentially on temperature, a small rise in temperature can lead to significant rise in vapor pressure, and consequently a corresponding increase in the flux of the AGMD system. The maximum recorded percentage increment in flux is about 730% when feed temperature increases from 40 °C to 80 °C at coolant temperature of 15 °C. It can also be noticed from Fig. 4 that the flux decreases with increasing coolant temperature. The observed reduction in permeate flux due to increasing coolant temperature is due to the reduction in the transmembrane driving force responsible for permeation. A maximum percentage reduction in permeate flux of about 31% was observed when the coolant temperature increases from 15 °C to 30 °C, at feed temperature of 40 °C.

Illustrated in Fig. 6 is the effect of feed inlet temperature on permeate flux at different feed flow rates. It can be seen that the flux increases with increasing feed flow rate. Increasing the feed flow rate promotes turbulence level in the flow channel and hence increases heat transfer coefficient in the feed boundary layer and reduces the effects of temperature and concentration polarizations. The maximum percentage increment in the permeate flux when the feed flow rate increases from 1 to 5 L/min is about 32% at feed temperature of 80 °C. The maximum distillate flux obtained from the AGMD system is 71.1 kg/m^2 hr at feed temperature of 80 °C, coolant temperature of 20 °C, feed flow rate of 5 L/min; coolant feed flow rate of 3 L/min, and air gap width of 3 mm. Fig. 7 depicts the impact of feed temperature on flux at different coolant flow rates. It can be observed that an insignificant change in flux is obtained when the coolant flow rate increases from 1 to 3.5 L/min. The maximum recorded percentage rise in flux was about 4% at feed temperature of 80 °C when the coolant flow rate was increased from 1 to 3.5 L/min. On the other hand, increasing cooling water flow rate leads to an increase in the cooling water heat transfer coefficient of the cooling surface, it is obvious from Fig. 7 that coolant flow rate has negligible effect on flux. The effect of coolant flow rate is marginal as far as the minimum flow rate needed to cool the condensate surface is maintained.

Another important operating parameter dominating the performance of AGMD is the air gap width. The influence of air gap thickness at different feed temperatures is presented in Fig. 8. The investigation is

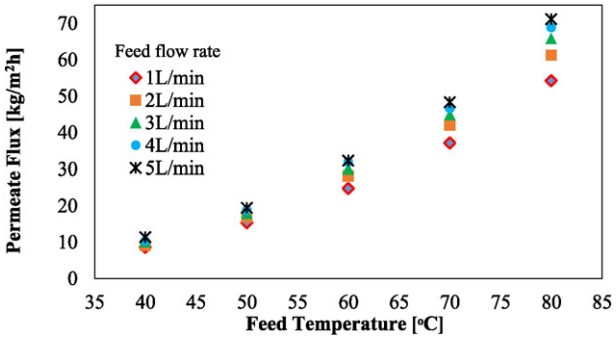

Fig. 6. Effect of feed temperature on flux at different feed flow rate. Test conditions: coolant temperature of 20 °C, coolant flow rate of 3 L/min, feed concentration of 75 mg/L, air gap width of 3 mm, and PTFE 0.45 μm membrane.

conducted using different air gap widths of 3, 5, and 7 mm at variable feed temperatures ranging from 40 to 80 °C. Decreasing the air gap width from 7 mm to 3 mm at a different feed inlet temperature leads to significant rise in permeate flux, particularly at higher feed temperatures. For example, reducing the air gap from 7 mm to 3 mm resulted in about 131% rise in the system flux at 40 °C feed temperature and about 100% increase in flux for feed temperature of 80 °C. Decreasing the air gap width implies reducing the resistance to mass transfer by reducing the vapor diffusion path length within the air gap compartment and increasing the driving transmembrane potential.

4.1.2. Effect of feed flow rate on permeate flux

The impact of feed flow rate on permeate flux at different coolant flow rates is presented in Fig. 9. An increase of about 32% in permeate flux was observed when feed flow rate increases from 1 to 5 L/min, approximately for all tested coolant flow rates. The permeate flux, however, increases by about 2% at feed flow rate of 5 L/min when coolant flow rate increases from 1 to 3.5 L/min. This observation indicates that the coolant flow rate is insignificant parameter to affect the flux of AGMD system. Fig. 9 illustrates the influence of feed flow rate at different coolant temperatures. Both feed flow rate and coolant temperature have relatively low influence on the system flux. According to results presented in Fig. 10, the observed percentage rise in permeate flux is about 30% when feed flow rate increases from 1 to 5 L/min, at a coolant temperature of 15 °C. Whereas the maximum percentage drop in the distillate production was about 13% when coolant temperature increases from 15 to 30 °C at 5 L/min feed flow rate.

4.1.3. Effect of coolant temperature on permeate flux

Fig. 11 shows the effect of coolant temperature on flux at different coolant flow rates. A maximum of 11% drop in permeate flux was

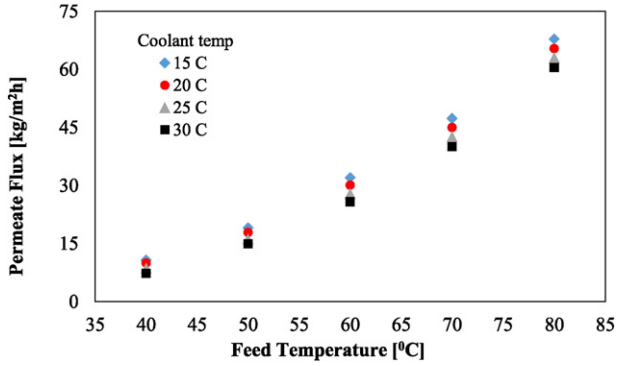

Fig. 5. Effect of feed temperature on flux at different coolant temperature. Test conditions: feed flow rate of 3 L/min, coolant flow rate of 3 L/min, feed concentration of 75 mg/L, air gap width of 3 mm, and PTFE 0.45 μm membrane.

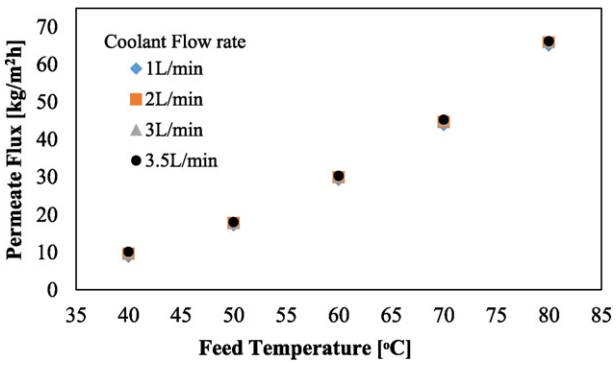

Fig. 7. Effect of feed temperature on flux at different coolant flow rate. Test conditions: coolant temperature of 20 °C, feed flow rate of 3 L/min, feed concentration of 75 mg/L, air gap width of 3 mm, and PTFE 0.45 μm membrane.

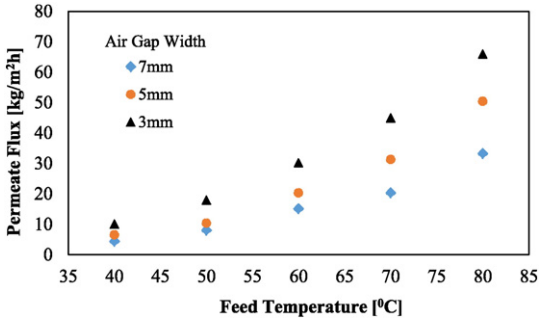

Fig. 8. Effect of air gap width on flux at different feed temperature. Test conditions: coolant temperature of 20 °C, feed flow rate of 3 L/min, coolant flow rate of 3 L/min, feed concentration of 75 mg/L, and PTFE 0.45 μm membrane.

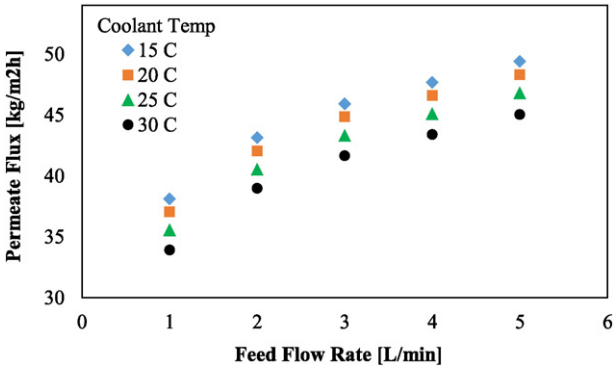

Fig. 10. Effect of feed flow rate on flux at different coolant temperature. Test conditions: feed temperature of 70 °C, coolant flow rate of 3 L/min, feed concentration of 75 mg/L, air gap width of 3 mm, and PTFE 0.45 μm membrane.

observed when coolant temperature increases from 15 to 30 °C at 1 L/min coolant flow rate, at feed temperature of 70 °C. The effect of coolant temperature on flux in this case is less significant compared with the effect of feed temperature or air gap width. As such, using cooling water at atmospheric condition is advisable in this context if the feed temperature is high enough. This will lower the cost of energy input for keeping the cooling water below the room temperature. Therefore, it is good to locate the MD plant near a water body where cooling water at atmospheric condition can be obtained. It can also be noticed in Fig. 11 that a maximum rise in flux of about 1.5% was recorded when the coolant flow rate increases from 1 L/min to 3.5 L/min at 15 °C coolant temperature. This result is consistent with previously discussed results in Figs. 7 and 9, which show that the effect of coolant flow rate on permeate flux is marginal.

4.1.4. Effect of membrane pore size on the AGMD permeate flux

The effect of membrane pore size on the permeate flux is investigated and presented in Figs. 12 to 14. Illustrated in Fig. 12 is the influence of membrane pore size on the flux at different feed temperatures and feed flow rates. In this investigation, two membranes with two different pore sizes (PTFE 0.45 μm and PTFE 0.22 μm) are tested. The rate of permeate flux obtained by using the PTFE 0.45 μm membrane is slightly higher compared to the case where the PTFE 0.22 μm membrane is used at different feed temperatures and feed flow rates. This is an indication that permeate flux increases with increasing membrane pore size, however, this increase is not linear function of the pore size. In addition, the membrane porosity of PTFE 0.45 μm is slightly greater than that of PTFE 0.22 μm as shown in Table 1, whereas the *LEP* of the membrane PTFE 0.45 μm is smaller than that of the membrane PTFE 0.22 μm. The PTFE 0.45 μm membrane recorded a maximum of about 13% rise in permeate flux over PTFE 0.22 μm membrane at 80 °C feed temperature and feed flow rate of 5 L/min. The effect of membrane pore size on the permeate flux at different feed temperature and coolant temperature is also investigated and presented in Fig. 13 were the permeate flux increases with increasing membrane pore size. A rise of about 12% in flux was recorded by PTFE 0.45 μm membrane over PTFE 0.22 μm membrane at 80 °C feed temperature and 15 °C coolant temperature. The PTFE 0.45 μm membrane recorded an increase of about 7% in permeate flux over that of the membrane PTFE 0.22 μm at 15 °C coolant temperature and feed flow rate of 5 L/min. It is important to state that the quality of permeate flux obtained using PTFE membrane is not affected by changing the pore size. The recorded salt rejection factor is 99.99%, using the two membranes.

It is of particular interest to examine the combined influence of pore size and air gap thickness on the flux, at different feed temperatures. Fig. 14 shows the flux production of two PTFE membranes with different pore sizes of 0.22 and 0.45 μm, under variable air gap width and feed temperature. The figure attests the fact that the effect of the tested pore sizes on flux is very small compared with the effect of the air gap width, and that the mass transfer resistance in the membrane due to the pore size is very small compared to that due to the air gap.

4.1.5. Effect of feed concentration on the AGMD performance

The effect of the concentration of feed water on the permeate flux is investigated at different feed temperatures, feed flow rates, and coolant temperatures. The tested feed solutions are distilled water (TDS of 0.075 g/L); laboratory prepared feed solutions with salt concentrations ranging from 4 to 50 g/L, and raw seawater (TDS of about 60 g/L). Each feed solution was tested at different feed temperatures ranging from 40 to 80 °C, feed flow rates ranging from 1 to 5 L/min and coolant temperature ranging from 15 to 30 °C. Depicted in Fig. 15 is the impact

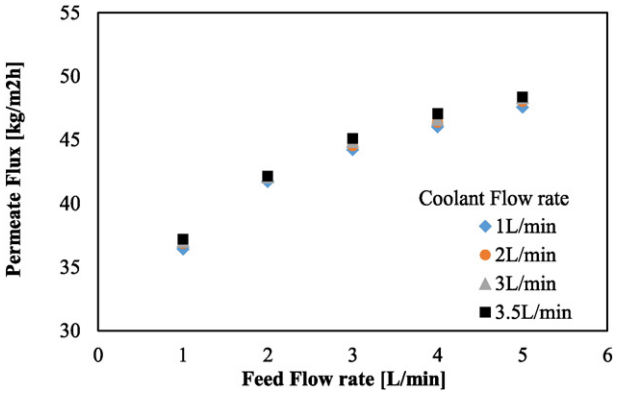

Fig. 9. Effect of feed flow rate on flux at different coolant flow rate. Test conditions: coolant temperature of 20 °C, feed temperature of 70 °C, feed concentration of 75 mg/L, air gap width of 3 mm, and PTFE 0.45 μm membrane.

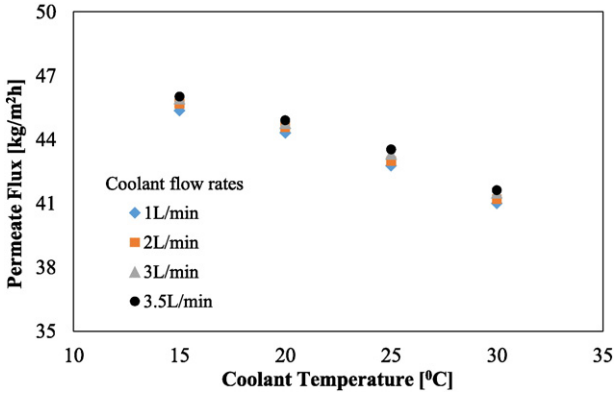

Fig. 11. Effect of coolant temperature on flux at different coolant flow rate. Test conditions: feed temperature of 70 °C, feed flow rate of 3 L/min, feed concentration of 75 mg/L, air gap width of 3 mm, and PTFE 0.45 μm membrane.

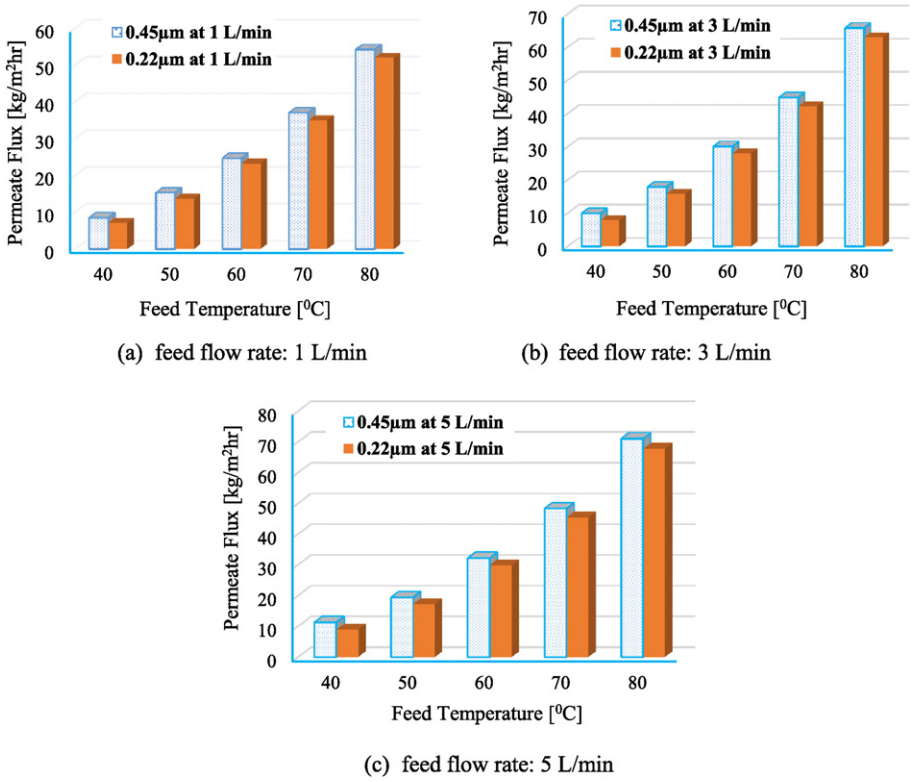

Fig. 12. Influence of the membrane pore size on flux at different feed flow rates. Test conditions: coolant temperature: 20 °C; coolant flow rate: 3 L/min; feed concentration: 75 mg/L; and air gap width: 3 mm. (a) Feed flow rate: 1 L/min. (b) Feed flow rate: 3 L/min. (c) Feed flow rate: 5 L/min.

of the feed salinity on the AGMD permeate flux at different feed temperatures. The permeate flux tends to decrease gradually with increasing feed salt concentration. The maximum and minimum percentage reduction in permeate flux when the feed concentration is increased from 0.075 g/L to 60 g/L is about 17% and 5% which corresponds to feed temperatures of 40 and 80 °C, respectively. The gradual reduction

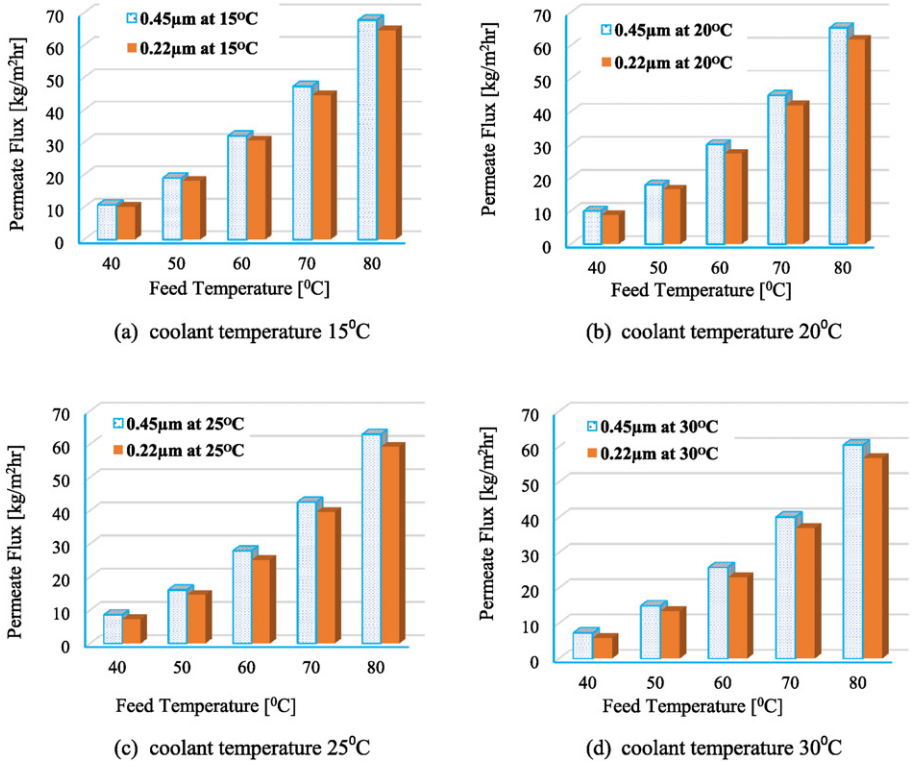

Fig. 13. Influence of the membrane pore size on permeate flux at different coolant temperatures. Test conditions: feed flow rate: 3 L/min; coolant flow rate: 3 L/min; feed concentration: 75 mg/L; and air gap width: 3 mm. (a) Coolant temperature 15 °C. (b) Coolant temperature 20 °C. (c) Coolant temperature 25 °C. (d) Coolant temperature 30 °C.

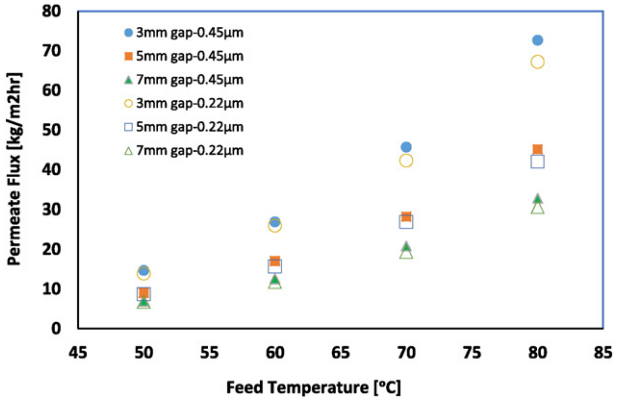

Fig. 14. Influence of the membrane pore size on permeate flux at different coolant temperatures. Test conditions: feed flow rate: 3 L/min; coolant flow rate: 3 L/min; coolant temperature: 20 °C, feed concentration: 1150 mg/L.

in the AGMD flux with increasing feed salinity is a direct result of increasing the effect of concentration polarization, which reduces water vapor pressure difference across the membrane. In general, the impact of feed concentration on the permeate flux is less significant compared to other membrane desalination technology like reverse osmosis where high feed salinity affects the performance of the system seriously. In most cases, the measured salt rejection factor is found to be 99.98% and above. The results indicate that working at higher feed temperatures is recommended because it provides lower percentage of flux reduction over the same range of feed concentrations.

The investigation of the effect of feed concentration on the permeate flux at different feed flow rates is presented in Fig. 16. Each feed concentration is tested at different feed flow rates ranging from 1 to 5 L/min at constant feed temperature and air gap width. It can be noticed that the system production rate decreases gradually with increasing the feed concentration. The maximum and minimum percentage reduction in permeate flux with the increasing salinity are 10% and 5% at 1 L/min and 5 L/min feed flow rate, respectively. The feed salinity has lesser impact on the permeate flux at high feed flow rates. This is because of higher turbulent levels achieved at higher flow rates, which reduces the effects of the concentration polarization.

The effect of the feed concentration on the permeate flux is also investigated at different coolant temperatures. Each feed concentration is tested at different coolant temperatures ranging from 15 to 30 °C under constant feed temperature, feed flow rate, and air gap width. Fig. 17 shows that the permeate flux decreases with increasing the salt concentration of the feed water. The maximum and minimum percentage drop in the permeate flux when the feed concentration increases from 0.075 g/L to 60 g/L is 10% and 7%, respectively, at a coolant temperature

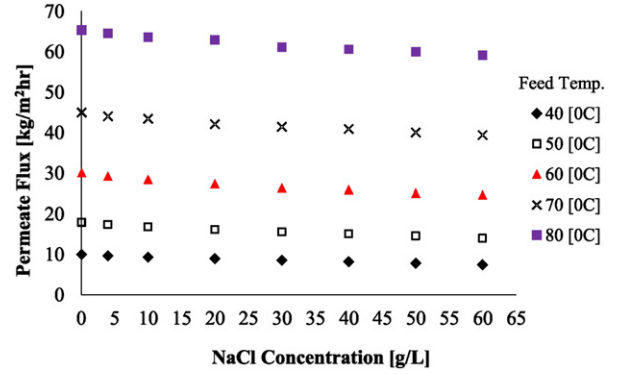

Fig. 15. Effect of feed concentration on permeate flux at different feed temperatures. Test conditions: coolant temperature: 20 °C; feed flow rate: 3 L/min; coolant flow rate: 3 L/min; air gap width: 3 mm, and PTFE 0.45 μm membrane.

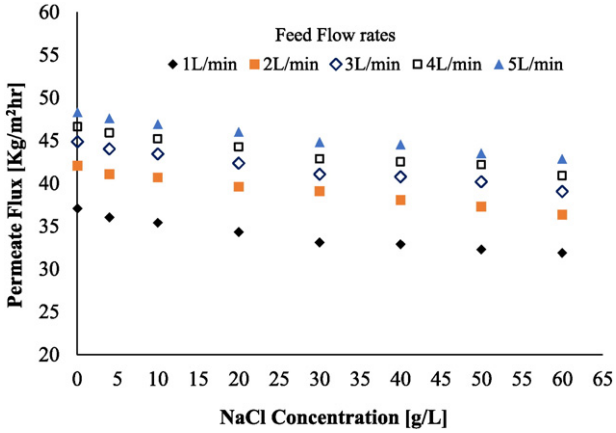

Fig. 16. Effect of feed concentration on flux at different feed flow rate. Test conditions: feed temperature: 70 °C; coolant temperature: 20 °C; coolant flow rate: 3 L/min; air gap width: 3 mm; and PTFE 0.45 μm membrane.

of 30 °C and 15 °C, respectively. One can observe that the effect of the feed concentration on the permeate flux is almost the same at lower and higher coolant temperature. However, since this effect is less at lower coolant temperature, it is therefore advisable to run the system at lower coolant temperature. In general, the AGMD performance slightly reduces with increasing the feed concentration. However, the impact is observed to be marginal when compared to other membrane desalination technology such as reverse osmosis. Hence, AGMD system can be used for desalination of highly concentrated seawater and brines.

4.1.6. Long term AGMD experiment

An experiment is conducted to investigate the degradation in flux due to continuous operation of the AGMD system. The experiment is run continuously without interruption for a total duration of 38 hours using a single PTFE 0.45 μm membrane sheet. Raw seawater obtained from Arabian Gulf sea, city of Khobar, Saudi Arabia, is used as a feed water. It is worth mentioning that the seawater is not subjected to any pre-treatment. External centrifugal pump is used to circulate the feed water from the heating bath. As shown in Fig. 18a, for the first 12 h of the experiment, the system production rate appears to be constant. After this period, the permeate flux begins to drop gradually (with little fluctuations) until the end of the experiment. A 27% reduction in the AGMD permeate flux is recorded after 38 h. The quality of the permeate flux against the experimental time is depicted in Fig. 18b and c. The permeate TDS increases with time from about 6 mg/L to 38 mg/L after 38 h of continuous

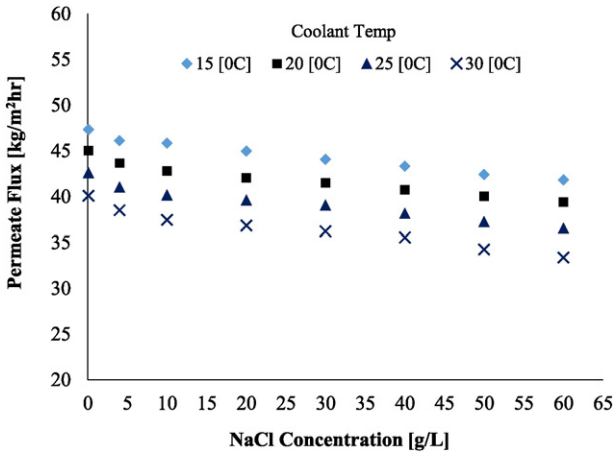

Fig. 17. Effect of the feed concentration on the permeate flux at different coolant temperatures. Test conditions: feed temperature: 70 °C; feed flow rate: 3 L/min; coolant flow rate: 3 L/min, air gap width: 3 mm, and PTFE 0.45 μm membrane.

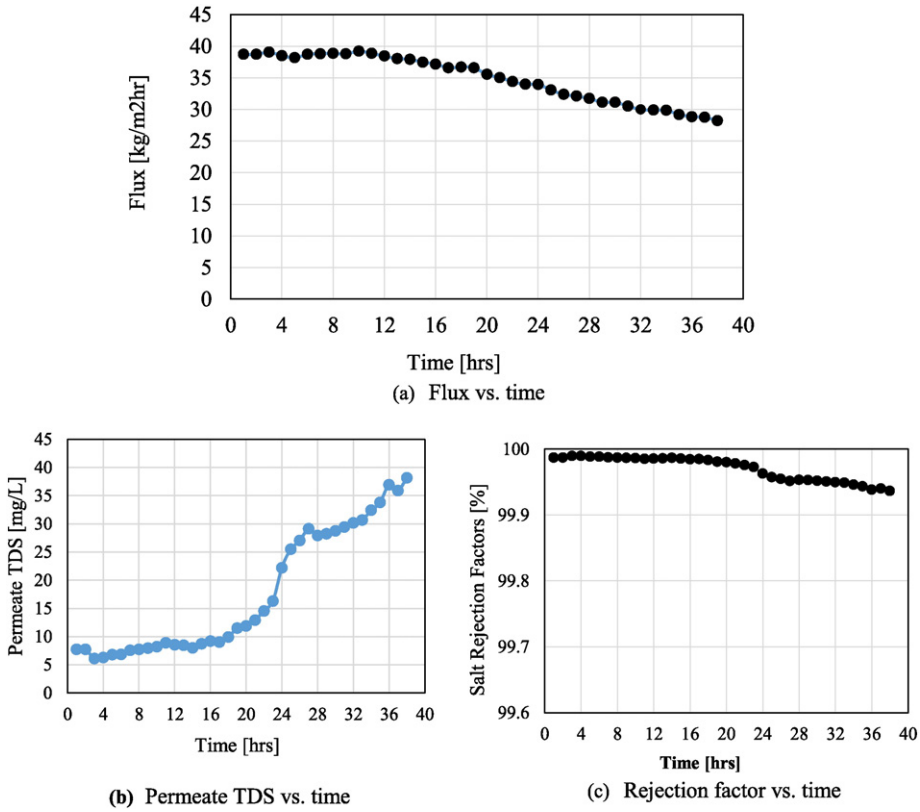

Fig. 18. Impact of the membrane operating time on the AGMD permeate flux, permeate concentration, and salt rejection factor. Test conditions: feed temperature: 70 °C; coolant temperature: 20 °C; feed flow rate: 3 L/min; coolant flow rate: 3 L/min; air gap width: 3 mm, and PTFE 0.45 μm membrane. (a) Flux vs. time. (b) Permeate TDS vs. time. (c) Rejection factor vs. time.

operation. A slight reduction in the calculated salt rejection factor is observed over the test duration. However, the salt rejection factor remains above 99.9%. It should be noted that the concentration of the feed water is maintained constant during all test duration by repeated makeup to feed tank. The permeate flux declines due to scaling and salt precipitations on the membrane surface. In addition, it was noticed that the external centrifugal pump discharges brown water when started, which indicates corrosion of the internal pump components. The corrosion problem is expected to increase with increasing the salt concentration of the feed water. The scaling of the rusty water on membrane surface with time is one of the causes to reduce the permeate flux.

4.2. Theoretical model: validation and results

In order to validate the developed theoretical model, comparisons are made between model results and the obtained experimental data at different operating parameters. The validation of the model results is presented in Fig. 19(a–d). Fig. 19a compares the theoretical model results and the experimental measurements of the permeate flux at different feed temperatures and different air gap widths for the PTFE 0.45 μm membrane, with feed concentration of 75 mg/L. The model is able to predict the permeate flux accurately at different feed temperatures with air gaps of 5 and 7 mm, where the calculated differences are approximately within 5%. The highest difference between the model prediction and the experimental permeate flux is measured for the small air gap of 3 mm width at the highest tested temperature of 80 °C. Fig. 19(a)–(d) show that the model predicts the permeate flux with a minimum error at 70 °C. Fig. 19(b)–(d) present the effects of the coolant temperature, the feed flow rate and the coolant flow rate on the AGMD permeate flux at three selected feed temperatures of 60, 70, and 80 °C. The data corresponding to the air gap width of 3 mm is selected for comparisons. The model is showing very good results compared to the experimental data at a feed temperature of 60 °C, and excellent agreement with experimental data at feed temperature of 70 °C. For the feed temperature 80 °C, the model is over-predicting the permeate flux with about 15% increase compared to the experimental values. It may be understood from Fig. 19 that the model results deviate more from experimental measurements for small gaps with high feed temperature. The observed over-prediction at small gap width and high feed temperature may be attributed to the high heat loss from the AGMD module; which is not considered in the theoretical model.

Fig. 20(a)–(d) shows the effect of the different operating conditions on the calculated thermal (evaporative) efficiency (*EE*), presented in Eq. (23), using the PTFE 0.45 μm membrane. The thermal efficiency represents the part of the heat that contributes to evaporation and production of permeate divided by total heat input in the membrane module [26]. *EE* is always lower than 100%. As shown in Fig. 19, the designed AGMD module exhibits *EE* values above 96.5%. *EE* increases from 96.8% to 99.2% when the feed temperature increases from 40 to 80 °C, see Fig. 20(a). At a higher feed temperature, *EE* is high because the vapor pressure is high and the heat loss by conduction is low. Careful observation of Fig. 20(b) reveals that *EE* tends to slightly increase with increasing the coolant temperature. From Fig. 20(a) and (b) it can be seen that the air gap width has no effect on *EE*. In addition, increasing the feed flow rate and the coolant flow rate has insignificant effects on *EE* as shown in Fig. 20(c) and (d). This is expected since for coolant flow rate has a marginal effect on the permeate flux. Since *EE* is mainly influenced by the feed temperature, it is therefore advisable to operate the AGMD system at high feed temperatures.

Drawbacks of the MD process include the effects of temperature and concentration polarizations. The influence of the concentration polarization on the reduction of the permeate flux is much smaller than that of the temperature polarization. The effects of the operating conditions on the temperature polarization coefficient (θ), defined earlier by Eq. (21), are shown in Fig. 21. It can be observed that θ slightly decreases with increasing the feed temperature, Fig. 21(a). This is because the

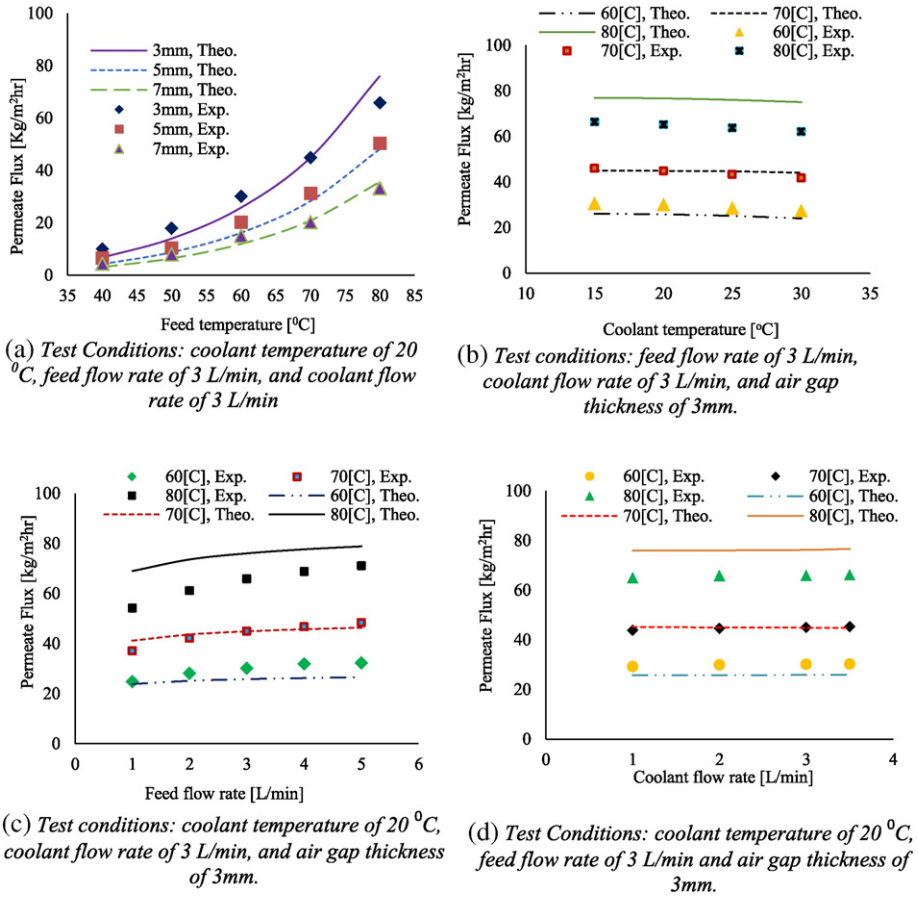

(a) *Test Conditions: coolant temperature of 20 °C, feed flow rate of 3 L/min, and coolant flow rate of 3 L/min*

(b) *Test conditions: feed flow rate of 3 L/min, coolant flow rate of 3 L/min, and air gap thickness of 3mm.*

(c) *Test conditions: coolant temperature of 20 °C, coolant flow rate of 3 L/min, and air gap thickness of 3mm.*

(d) *Test Conditions: coolant temperature of 20 °C, feed flow rate of 3 L/min and air gap thickness of 3mm.*

Fig. 19. Model validation at different operating parameters. (a) Test conditions: coolant temperature of 20 °C, feed flow rate of 3 L/min, and coolant flow rate of 3 L/min. (b) Test conditions: feed flow rate of 3 L/min, coolant flow rate of 3 L/min, and air gap thickness of 3 mm. (c) Test conditions: coolant temperature of 20 °C, coolant flow rate of 3 L/min, and air gap thickness of 3 mm. (d) Test conditions: coolant temperature of 20 °C, feed flow rate of 3 L/min and air gap thickness of 3 mm.

higher permeate fluxes produced by the higher vapor pressure difference is compensated by the increase of the heat transfer by conduction. Values of θ also tends to slightly decrease with increasing the coolant temperature as shown in Fig. 21(b), due to the reduction in transmembrane potential. However, the rate of reduction in θ is small when compared to the effect of the feed temperature on θ. The effect of the air gap width on temperature polarization is evident. Smaller air gap width leads to lower θ values. However, it can be noticed that θ increases with increasing the feed flow rate, Fig. 21(c). The percentage increment in θ is about 10% when the feed flow rate increases from 1 to 5 L/min. The rise in θ with increasing feed flow rate is attributed to increasing flow turbulence level in the feed channel, which results in better mixing of feed solution thereby decreasing the feed boundary layer resistance (smaller difference between the feed water temperature and membrane surface temperature- feed side). Increasing the coolant flow rate leads to negligible change in θ as shown in Fig. 21(d).

5. Conclusions

Comprehensive experimental and theoretical studies of the performance of air gap membrane distillation (AGMD) system are presented. The effect of the AGMD operating parameters such as feed inlet temperature, feed flow rate, coolant temperature, coolant flow rate, feed concentration, membrane pore size, and the air gap width on the permeate flux have been investigated. The results of the theoretical model are compared and validated against the experimental data. The variation of the evaporative efficiency of the AGMD module and the temperature polarization coefficient are thoroughly investigated at different operating parameters. The permeate flux increases with the feed temperature and the feed flow rate. However, it decreases with increasing the air gap width and the coolant temperature. Increasing the coolant flow rate tends to marginally increase the flux. The feed temperature is the most influential factor affecting the AGMD performance, where the permeate flux increases exponentially with the feed temperature. For example, an increase between 550 to 750% in permeate flux is recorded when the feed temperature is increased from 40 °C to 80 °C, depending on the other operating variables. The other dominant operating parameter affecting the permeate flux considerably is the air gap width. A maximum of 132% rise in permeate flux is observed when it was decreased from 7 to 3 mm. The effects of the feed flow rate and the coolant temperature are relatively small compared to that of the feed temperature and the air gap width. Meanwhile, the effect of the coolant flow rate on the AGMD flux is marginal or negligible within the tested range. The PTFE membrane having 0.45 μm pore size results in 11% rise in permeate flux over the membrane PTFE 0.22 μm when the feed temperature increases from 40 °C to 80 °C. However, there is no clear difference in the quality (TDS) of the permeate produced using the two membranes. Long term experiment was conducted using raw seawater without pre-treatment for 38 h of continuous operation of the system. The permeate flux tends to decrease with time mainly due to scaling and concentration polarization effects. Increasing the feed concentration from 0.075 to 60 g/L led to an average reduction in the measured permeate flux of 11% at different feed temperatures.

The theoretical model for predicting the permeate flux is proven to be valid. The theoretical values of the permeate flux are within 0 to 15% of the experimentally measured values. The module evaporative efficiency increases significantly with increasing the feed temperature due to the higher evaporation rate, higher vapor pressure, and minimum conduction heat loss. The evaporation efficiency also increases with increasing the coolant temperature and the feed

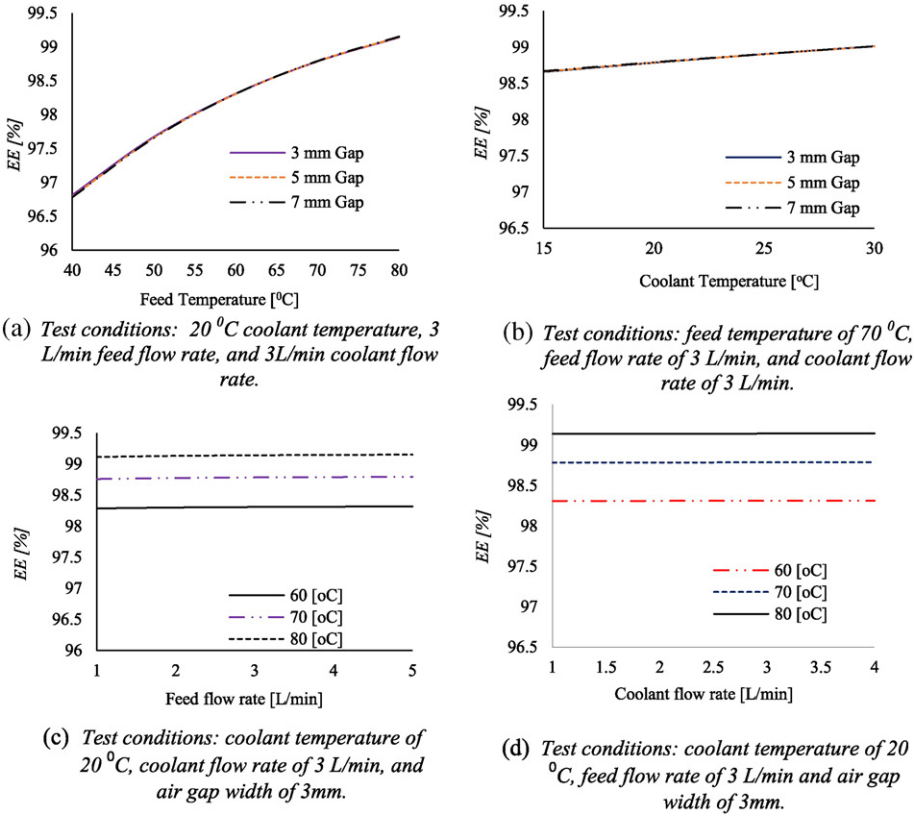

Fig. 20. Variation of evaporative (thermal) efficiency, *EE*, at different operating parameters. (a) Test conditions: 20 °C coolant temperature, 3 L/min feed flow rate, and 3 L/min coolant flow rate. (b) Test conditions: feed temperature of 70 °C, feed flow rate of 3 L/min, and coolant flow rate of 3 L/min. (c) Test conditions: coolant temperature of 20 °C, coolant flow rate of 3 L/min, and air gap width of 3 mm. (d) Test conditions: coolant temperature of 20 °C, feed flow rate of 3 L/min and air gap width of 3 mm.

flow rate while it seems unaffected by increasing the coolant flow rate. The temperature polarization coefficient decreases with increasing the feed and coolant temperatures. However, it increases with the feed flow rate.

Nomenclature

Symbols

b	air gap thickness [m]
C_p	specific heat [kJ/kg·K]
D_h	flow channel hydraulic diameter [m]
D_{wa}	diffusion coefficient of water vapor in air [m^2/s]
EE	evaporation (thermal) efficiency %
g	gravitational acceleration [m/s^2]
h	Heat transfer coefficient [W/m^2·K]
h_d	condensate film heat transfer coefficient [W/m^2·K]
H_w	enthalpy of vaporization [kj/kg]
J_w	permeate flux [kg/m^2·s]
K	thermal conductivity [W/m·k]
ι	thickness of the cooling plate [m]
L	height of the cooling plate [m]
B_w	Mass transfer coefficient [kg/m^2·hr·Pa]
Nu	Nusselt number
P	total pressure [Pa]
P_v	vapor pressure [Pa]
P_a	air pressure [Pa]
Pr	Prandtl number
Q_s	sensible heat transfer [W/m^2]
Q_v	vaporization heat transfer [W/m^2]
Q_c	conduction heat transfer [W/m^2]
R	gas constant [J/K·mol]
Re	Reynolds number
T	absolute temperature [K]
V	velocity of water in channel [m/s]
T_f	bulk feed temperature
T_{mf}	temperature at feed side membrane
T_{mp}	temperature at coolant side membrane
T_{cd}	temperature at the condensate
T_{pa}	temperature of condensation plate-air gap side
T_{pc}	temperature at condensation plate-coolant side
Tc	bulk coolant temperature

Subscripts and superscripts

a	air
w	water
f	feed
m	membrane
b	bulk
mf	feed side of membrane
mp	coolant side of membrane

Greek letters

δ	membrane thickness; film thickness [m]
ε	porosity
τ	tortuosity
μ	viscosity [N·s/m^2]
ρ	density [kg/m^3]
θ	temperature polarization

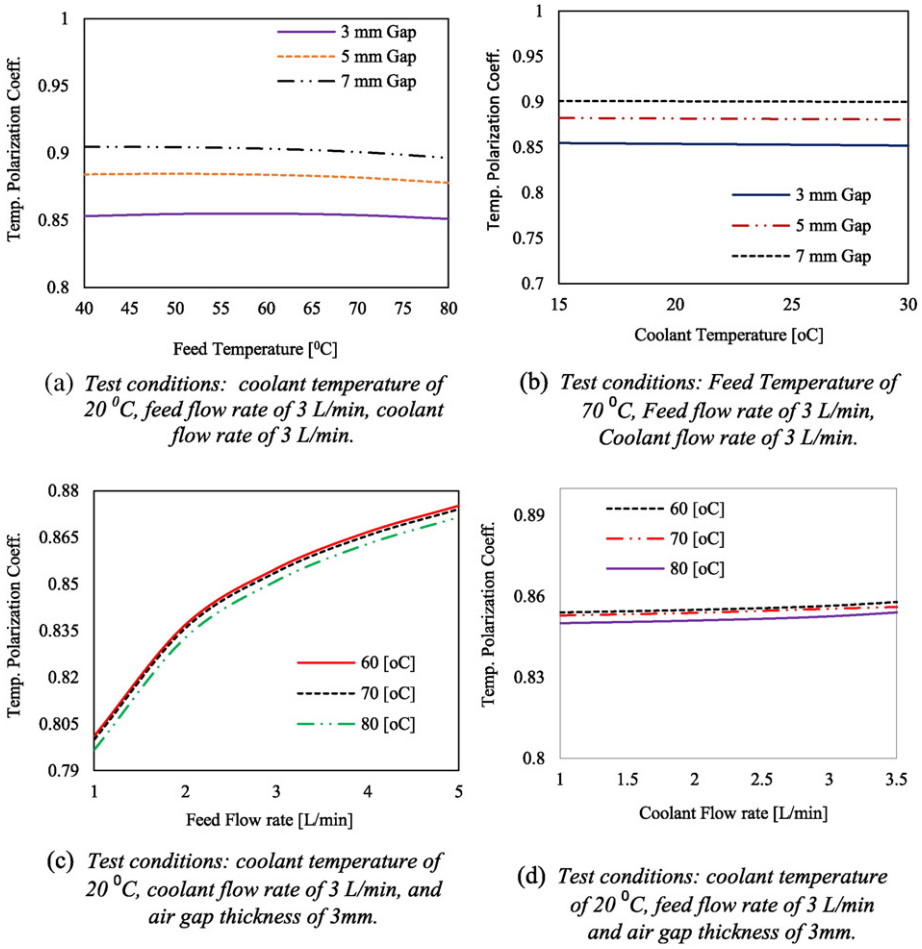

Fig. 21. Temperature polarization coefficient at different operating parameters. (a) Test conditions: coolant temperature of 20 °C, feed flow rate of 3 L/min, coolant flow rate of 3 L/min. (b) Test conditions: feed temperature of 70 °C, feed flow rate of 3 L/min, coolant flow rate of 3 L/min. (c) Test conditions: coolant temperature of 20 °C, coolant flow rate of 3 L/min, and air gap thickness of 3 mm. (d) Test conditions: coolant temperature of 20 °C, feed flow rate of 3 L/min and air gap thickness of 3 mm.

Acknowledgments

The authors acknowledge the support received from King Fahd University of Petroleum & Minerals (KFUPM) to complete this research work under the funded project # IN121043.

References

[1] M.A. Dawoud, The role of desalination in augmentation of water supply in GCC countries, Desalination 186 (2005) 187–198.
[2] M. Khayet, T. Matsuura, Membrane Distillation Principles and Applications, Elsevier, B.V., 2011
[3] M.N.A. Hawlader, R. Bahar, K.C. Ng, L.J.W. Stanley, Transport analysis of an air gap membrane distillation (AGMD) process, Desalin. Water Treat. 42 (2012) 333–346.
[4] B.L. Pangarkar, M. Sane, Performance of air gap membrane distillation for desalination of ground water and seawater. Word academy of science, Eng. Technol. 5 (2011) 03–26.
[5] D. Singh, K.K. Sirkar, Desalination by air gap membrane distillation using a two hollow-fiber-set membrane module, J. Membr. Sci. 421-422 (2012) 172–179.
[6] R. Tian, H. Gao, X.H. Yang, S.Y. Yan, S. Li, A new enhancement technique on air gap membrane distillation, Desalination 332 (2014) 52–59.
[7] A. Khalifa, Water and air gap membrane distillation for water desalination—an experimental comparative study, Sep. Purif. Technol. 141 (2015) 276–284.
[8] L. Francis, N. Ghaffour, A. Alsaadi, G. Amy, Material gap membrane distillation: a new design for water vapor flux enhancement, J. Membr. Sci. 448 (2013) 240–247.
[9] M. Essalhi, M. Khayet, Application of a porous composite hydrophobic/hydrophilic membrane in desalination by air gap and liquid gap membrane distillation: a comparative study, Sep. Purif. Technol. 133 (2014) 176–186.
[10] R. Bahar, M.N.A. Hawlader, T.F. Ariff, Channeled coolant plate: a new method to enhance freshwater production from an air gap membrane distillation (AGMD) desalination unit, Desalination 359 (2015) 71–81.
[11] D.U. Lawal, A.E. Khalifa, Flux prediction in direct contact membrane distillation, Int. J. Mater. Mech. Manuf. 2 (4) (2014) 302–308.
[12] Dahiru U. Lawal, Atia E. Khalifa, Experimental investigation of an air gap membrane distillation unit with double-sided cooling channel, Desalination and Water Treatment (May 2015) http://dx.doi.org/10.1080/19443994.2015.1042065.
[13] U. Dehesa-Carrasco, C.A. Pérez-Rábago, C.A. Arancibia-Bulnes, Experimental evaluation and modeling of internal temperatures in an air gap membrane distillation unit, Desalination 326 (2013) 47–54.
[14] A.S. Alsaadi, N. Ghaffour, J.D. Li, S. Gray, L. Francis, H. Maab, G.L. Amy, Modeling of air-gap membrane distillation process: a theoretical and experimental study, Desalination, J. Membr. Sci. 445 (2013) 53–65.
[15] H. Geng, H. Wu, P. Li, Q. He, Study on a new air-gap membrane distillation module for desalination, Desalination 334 (2014) 29–38.
[16] A.S. Jonsson, R. Wimmerstedt, A.C. Harrysson, Membrane distillation-A theoretical study of evaporation through microporous membranes, Desalination 56 (1985) 237–249.
[17] F.A. Banat, J. Simandl, Desalination by membrane distillation: a parametric study, Sep. Sci. Technol. 33 (2) (1998) 201–226.
[18] S. Kimura, S. Nakao, Transport phenomena in membrane distillation, J. Membr. Sci. 33 (1987) 285–298.
[19] A. Alkhudhiri, N. Darwish, N. Hilal, Membrane distillation: a comprehensive review, Desalination 287 (2012) 2–18.
[20] A. Alkhudhiri, N. Darwish, N. Hilal, Treatment of high salinity solutions: application of air gap membrane distillation, Desalination 287 (2012) 55–60.
[21] G.L. Liu, C. Zhu, C.S. Cheung, C.W. Leung, Theoretical and experimental studies on air gap membrane distillation, Heat Mass Transf. 34 (4) (1998) 329–335.
[22] R.B. Bird, W.E. Stewart, E.N. Lightfoot, Transport Phenomena, second ed. Wiley, New York, 2002.
[23] F.A. Banat, Membrane Distillation for Desalination and Removal of Volatile Organic Compounds From Water(PhD Thesis) McGill University, Montreal, Canada, 1994.
[24] J. Phattaranawik, R. Jiraratananon, A.G. Fane, Effect of pore size distribution and air flux on mass transport in direct contact membrane distillation, J. Membr. Sci. 215 (2003) 75–85.
[25] K. Smolders, A.C.M. Franken, Terminology for membrane distillation, Desalination 72 (1989) 249–262.
[26] M. Khayet, A. Velazquez, J.I. Mengual, Modelling mass transport through a porous partition: effect of pore size distribution, J. Non-Equilib. Thermodyn. 29 (2004) 279–299.

[27] M. Khayet, Membranes and theoretical modeling of membrane distillation: a review, Adv. Colloid Interf. Sci. 164 (2011) 56–88.
[28] M. Khayet, T. Matsuura, J.I. Mengual, Porous hydrophobic/hydrophilic composite membranes: estimation of the hydrophobic layer thickness, J. Membr. Sci. 266 (2005) 68–79.
[29] M. Khayet, A. Velazquez, J.I. Mengual, Modelling mass transport through a porous partition: effect of pore size distribution, J. Non-Equilib. Thermodyn. 29 (2004) 279–299.
[30] M. Khayet, T. Matsuura, J.I. Mengual, Porous hydrophobic/hydrophilic composite membranes: estimation of the hydrophobic layer thickness, J. Membr. Sci. 266 (2005) 68–79.
[31] M. Essalhi, M. Khayet, Self-sustained webs of polyvinylidene fluoride electrospun nanofibers at different electrospinning times: 2. Theoretical analysis, polarization effects and thermal efficiency, J. Membr. Sci. 433 (2013) 180–191.
[32] Ó. Andrjesdóttir, C. Ong, M. Nabavi, S. Paredes, A. Khalil, B. Michel, D. Poulikakos, An experimentally optimized model for heat and mass transfer in direct contact membrane distillation, Int. J. Heat Mass Transf. 66 (November 2013) 855–867.
[33] D.U. Lawal, Desalination Using Air Gap Membrane Distillation(MSc. Thesis) King Fahd University of Petroleum and Minerals, 2014.